Food Chemistry 413 (2023) 135675

Contents lists available at ScienceDirect

Food Chemistry

journal homepage: www.elsevier.com/locate/foodchem

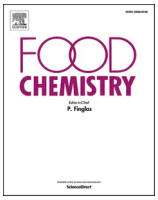

Preparation of cellulose nanofibers from potato residues by ultrasonication combined with high-pressure homogenization

Xiaowen Liu [a,1], Hongnan Sun [a,*,1], Taihua Mu [a,*], Marie Laure Fauconnier [b], Mei Li [c]

[a] Laboratory of Food Chemistry and Nutrition Science, Institute of Food Science and Technology, Chinese Academy of Agricultural Sciences, Key Laboratory of Agro-Products Processing, Ministry of Agriculture and Rural Affairs, No. 2 Yuan Ming Yuan West Road, Haidian District, P.O. Box 5109, Beijing 100193, China
[b] Laboratory of Chemistry of Natural Molecules, University of Liege, Gembloux Agro-Bio Tech, Passage des Déportés 2, 5030 Gembloux, Belgium
[c] Gansu Innovation Center of Fruit and Vegetable Storage and Processing, Agricultural Product Storage and Processing Research Institute, Gansu Academy of Agricultural Sciences, Lanzhou 730070, China

ARTICLE INFO

Keywords:
Cellulose nanofibers
Morphology
Structure
Thermal stability
Rheological behavior

ABSTRACT

In this study, the preparation parameters of cellulose nanofibers from potato residues (PCNFs) by ultrasonication combined with high-pressure homogenization were optimized based on yield, zeta-potential and morphology. The optimal parameters were as follows: ultrasonic power of 125 W for 15 min and homogenization pressure of 40 MPa four times. The yield, zeta potential and diameter range of the obtained PCNFs were 19.81 %, −15.60 mV and 20–60 nm, respectively. Fourier transform infrared spectroscopy, X-ray diffraction and nuclear magnetic resonance spectroscopy results showed that part of the crystalline region of cellulose was destroyed, resulting in a decrease in crystallinity index from 53.01 % to 35.44 %. The maximum thermal degradation temperature increased from 283 °C to 337 °C. PCNFs suspensions were non-Newtonian fluids and exhibited rigid colloidal particle properties. In conclusion, this study provided alternative uses for potato residues generated from starch processing and showed great potential for various industrial applications of PCNFs.

1. Introduction

Potatoes (*Solanum tuberosum* L.) are the fourth largest crop in the world after maize, wheat and rice (Waliullah, Mu, & Ma, 2021). China ranks first in global potato production, with 78 million tons processed in 2020, accounting for 21.79 % of the world's total potato production (FAO, 2022). Potatoes are rich in nutritional and functional components, such as starch, protein, dietary fiber, vitamins and minerals. Currently, potatoes play an important role in food security, particularly in poor areas, where many people still lack food security (Wijesinha--Bettoni & Mouille, 2019).

In China, the main potato products are starch and starch noodles. The potato residues are the by-products of potato starch processing. In particular, about 3 million tons of wet residues are produced annually (Waliullah et al., 2021). So far, only a small amount of potato residues are utilized as cheap animal feed, and most of them are thrown away, resulting in serious resource waste and environmental pollution. Therefore, searches for applications of potato residues are helpful to save resources and solve environmental problems. Several previous studies have investigated the dietary fiber in potato residues and have characterized its structural, physicochemical and functional properties (Ma et al., 2022; Scharf et al., 2020; Waliullah et al., 2021). Potato residues are rich in cellulose, and thus, can be used as high-quality raw material for preparing cellulose nanofibers (CNFs).

CNFs are nanoscale derivatives of cellulose. CNFs consist of 1000 to 10,000 molecules of linear homopolysaccharide composed of β-D-glucopyranose units linked together by β-1–4-linkages (Xie et al., 2016). CNFs can be produced from a variety of crop residues such as sugarcane bagasse agrowaste (Hongrattanavichit & Aht-Ong, 2020) and flaxseed fiber (Azhar et al., 2021). CNFs have attracted considerable interest owing to their notable properties such as high specific surface area (Dilamian & Noroozi, 2019), high aspect ratio, high Young's modulus, low cost, light weight, abundance, renewability and biodegradability (Li et al., 2015). CNFs have been used in various applications such as pharmaceutical and biomedical products (Pandey, 2021), and the controlled release of anticancer drugs (Kumari & Meena, 2021).

For efficiency, CNFs are traditionally prepared by some typical chemical methods, such as acid or alkaline hydrolysis, carboxyl

* Corresponding authors.
E-mail addresses: honey0329@163.com (H. Sun), mutaihua@126.com (T. Mu).
[1] These authors contributed equally.

https://doi.org/10.1016/j.foodchem.2023.135675
Received 1 September 2022; Received in revised form 9 February 2023; Accepted 9 February 2023
Available online 13 February 2023

methylation and TEMPO-mediated oxidation (Serra et al., 2017). Concentrated sulfuric acid hydrolysis is one of the most popular chemical methods to produce CNFs. Several adverse effects regarding concentrated sulfuric acid hydrolysis have been reported, such as environmental pollution, chemical residues, safety issues and equipment corrosion. Moreover, the suspension after hydrolysis needs to be diluted 10 times with deionized water to stop the reaction, which is water-consuming (Hongrattanavichit et al., 2020), further resulting in high energy consumption in the drying process. Arvidsson et al. (2015) compared the cumulative energy demand of three production routes for CNFs made from wood pulp. The three production routes are (1) the enzymatic production route, which includes an enzymatic pretreatment followed by microfluidization, (2) the carboxymethylation route, which includes a carboxymethylation pretreatment followed by microfluidization and (3) one step homogenization without pretreatment, here called the no pretreatment route. The results showed that CNFs produced via the carboxymethylation route clearly have the highest cumulative energy demand (1800 MJ kg^{-1}), whereas the enzymatic and no pretreatment routes both have lower cumulative energy demands (about 200 MJ kg^{-1}). In addition, CNFs prepared by mechanical methods are more conducive to modification, showing better thermal stability and higher viscoelastic and rheological stability even at lower concentrations (Michelin et al., 2020). High-pressure homogenization is one of the most popular mechanical methods used to prepare CNFs (Hamawand et al., 2020). Widiarto et al. (2019) prepared CNFs from cassava peel using a homogenizer and ultrasonication disruption procedure and compared those with CNFs obtained using a common acid hydrolysis procedure. Their results showed that the physical treatments can be used to successfully produce CNFs. Dilamian and Noroozi (2019) prepared CNFs from rice straw by chemical pretreatment with a high-shear speed homogenizer and high-intensity ultrasonication processes. However, potato residues are still not used as raw material for the preparation of CNFs.

The present study aimed to convert the residues generated during potato starch processing to CNFs by ultrasonication along with high-pressure homogenization. The preparation parameters were optimized based on the yield, zeta potential, morphology and diameter distribution of the CNFs. The CNFs obtained under the optimal preparation parameters were characterized using a rheometer as well as atomic force microscopy (AFM), transmission electron microscopy (TEM), zeta potential, Fourier transform infrared (FTIR) spectroscopy, X-ray diffraction (XRD), nuclear magnetic resonance (NMR) spectroscopy and thermogravimetric analysis (TGA).

2. Materials and methods

2.1. Materials

Potato residues supplied by Zhuanglang Hongda Starch Processing Co., Ltd (Pingliang, Gansu Province, China) were ground using a crusher (ZK-35A, Zhong KeHao Technology Development Co., Ltd, Beijing, China) and then sieved through a 0.15 mm (100 mesh) sieve. NaOH, H_2O_2 and thermostable α-amylase were obtained from Beijing Tongguang Fine Chemicals Co. (Beijing, China), Sinopharm Chemical Reagent Co., Ltd (Shanghai, China) and Beijing Solarbio Science & Technology Co., Ltd (Beijing, China), respectively. CNFs prepared by the mechanical method (high-pressure homogenization) (M-CNFs, diameter: 10–20 nm, length: 2–10 μm) were obtained from Tianjin Woodelfbio Co., Ltd (Tianjin, China), and those prepared by TEMPO-mediated oxidation (TEMPO-CNFs, diameter: 10–50 nm, length: 10–20 μm) were obtained from Zhejiang JinJiaHao Green Nanocellulose Co., Ltd, (Quzhou, Zhejiang Province, China). This study used deionized water.

2.2. Analysis of the approximate composition of potato residues

The approximate composition of the potato residues was determined. The starch content was determined using a Total Starch Assay Test Kit (Megazyme, Bure Ireland). The moisture was determined by referring to AOAC Methods of Analysis 930.15 (AOAC Official Method, 1999). Briefly, triplicates of potato residue samples were oven-dried at 103 °C for 72 h, transferred to a desiccator and allowed to cool to room temperature. The sample weights were recorded on a digital balance. The fat content was determined by referring to AOAC Methods of Analysis 954.02 (AOAC Official Method, 1999). Briefly, the 2 g potato residues were accurately weighed and put into a Mojonnier fat-extraction tube. The fat of potato residues was extracted using ethyl ether. The ethyl ether was collected in constant-weight beakers and was evaporated in a steam bath. The beakers were dried, cooled to room temperature in a desiccator and weighed immediately. The protein content was determined referring to AOAC Methods of Analysis 976.05 (AOAC Official Method, 1999), with a nitrogen-to-protein conversion factor of 6.25. The ash content was determined referring to AOAC Methods of Analysis 942.05 (AOAC Official Method, 1999), by weighing potato residue samples before and after heat treatment (600 °C for 2 h). The dietary fiber content was determined by referring to AOAC Methods of Analysis 991.43 (AOAC Official Method, 1999). The dietary fiber composition was determined following the method of Ma et al. (2015). Briefly, 2 g potato residues of dietary fiber were extracted with 0.25 % ammonium oxalate solution at 1:10 (w/v) for 2 h at 90 °C, followed by centrifugation. The process was performed three times, the supernatants were pooled, dialyzed and lyophilized to obtain pectin (C_1). After pectin extraction, the resulting residues were washed twice with 80 % (v/v) ethanol and three times with distilled water and lyophilized. The lyophilized residues were extracted twice with 4 M KOH and 0.1 % sodium borohydride at room temperature for 18 h. The residue (C_3) was filtered, washed with ethanol and distilled water, and lyophilized. The filtrates were collected, dialyzed and lyophilized to obtain hemicelluloses (C_2). C_3 residues were extracted with 72 % (v/v) H_2SO_4 at 4 °C for 24 h and filtered. The precipitate was washed with ethanol and distilled water, and freeze-dried to obtain C_4. The ash content (C_5) of the lyophilized precipitate was determined according to AOAC 942.05 (AOAC Official Method, 1999). The lignin and cellulose contents were C_4–C_5 and C_3–C_4–C_5, respectively. The results are shown in Table S1.

2.3. Preparation of CNFs

In this study, potato residue CNFs (PCNFs) were prepared using ultrasound combined with high-pressure homogenization. The effects of ultrasonic time, ultrasonic power, high-pressure homogenization cycles and high-pressure homogenization pressure on the yield, zeta potential, morphology and diameter distribution of the PCNFs were evaluated.

To remove starch fully, 5 g of potato residues were combined with deionized water (1:6, w/v), and the mixture was boiled for 3 min to completely gelatinize the starch. Then, 50 mL deionized water was immediately added followed by 600 μL thermostable α-amylase (KNu > 130 B/g). The sample then underwent ultrasonic treatment (JY92-IIN, Scientz, Zhejiang, China) followed by 7,500*g* centrifugation (GL-21M, Shanghai LuXiangyi Centrifuge Instrument Co., Ltd, Shanghai, China) for 10 min to remove the supernatant. Afterward, NaOH (7 %, w/v) was added to the sediment and incubated at 70 °C for 1.0 h, then centrifuged again to remove hemicellulose. Next, H_2O_2 (10 %, v/v) was added to the sediment, which was held for 1.5 h at 70 °C to remove the lignin. Finally, the suspension was washed with deionized water until neutral pH was reached, and the sediment was dried in an oven at 55 °C for 5 h to obtain the cellulose.

The cellulose was dispersed in deionized water and stirred with a magnetic stirrer (HJ-6, Changzhou Zhongbei Instrument Co., Ltd, Changzhou, China) for 3 h to prepare a 0.2 % (w/v) cellulose suspension. To avoid clogging during homogenization, the suspension was first treated with ultrasonic (JY92-IIN, Scientz) for 10 min at a power of 500 W followed by high-shear mulser shearing for 1 min at 10,000 rpm (I25, IKN Co., Ltd, Shanghai, China) to obtain a homogeneous cellulose

suspension. Then, the suspension was homogenized (D-3L, PhD Technology, St. Paul, MN, USA) to obtain the final PCNF suspension.

To optimize the preparation parameters of PCNFs, the effects of different time and powers of the ultrasonic treatment in the cellulose preparation procedure, and different homogenization cycles and pressure in the PCNFs preparation procedure on the yield, zeta potential and morphology of PCNFs were compared, and the optimal parameters were selected (Table S2).

The yield was calculated with Eq. (1):

$$\text{Yield}\,(\%) = M_P/M_{pr} \times 100, \quad (1)$$

where M_P was the weight of PCNFs and M_{pr} was the weight of potato residues.

The PCNFs were prepared under the optimal parameters and were freeze-dried to obtain a solid powder for easy preservation. All experiments in this study used powder CNFs.

2.4. Characterization of PCNFs

2.4.1. Zeta potential

The zeta potential was obtained following the method of Xu et al. (2021) with some modifications. The CNFs suspensions were diluted to 0.1 % (w/v) concentration with deionized water, the suspensions were transferred into a 1 mL zeta potential cell and the measurements were performed in 2 min with a Zetasizer Nano ZS (Malvern, Worcestershire, England). The measurements of every sample were repeated in quintuplicate.

2.4.2. Morphology

2.4.2.1. AFm. The PCNFs' morphologies were observed with an atomic force microscope (NX10, Park Systems, Suwon, South Korea) equipped with a PPP-NCHR probe (length, 125 μm, mean width, 30 μm, thickness, 4 μm) having a nominal spring constant of 42 N m^{-1} and a resonance frequency of 330 kHz, and an NCM head mode. Briefly, 30 μL of the suspension at 0.1 % (w/v) was applied to coat mica flakes, which were dried overnight to obtain the specimen. The AFM image (256 pxl × 256 pxl) was obtained according to the fast scan direction from left to right and the slow scan direction from top to bottom with a 0.56 Hz scan rate.

The diameter measurements were carried out following the method of Zai et al. (2022) with some modifications. For each sample, three AFM images were obtained and the AFM images were used to observe the morphologies of CNFs. The diameter distribution of CNFs was measured using ImageJ software (Image J win-64). The measurements were performed in triplicate. Briefly, the distance in pixels, known distance and the unit of the scale were inputted, and 150 fibers were counted randomly for each image. The diameters of selected CNFs were provided automatically by the software.

2.4.2.2. TEm. A 0.1 % (w/v) suspension was used to coat a copper grid, which was dried at room temperature. The samples were imaged under 120 kV using a manual emission transmission electron microscope (New Bio-TEM H-7500, Hitachi, Japan).

2.4.3. FTIR analysis

FTIR analysis was conducted following the method of Masruchi et al. (2018) with some modifications. The CNFs were mixed with dry KBr powder (1:150) and were ground completely in an agate mortar. The mixture was pressed with a hydraulic press at a pressure of 10 MPa for 30 s until a uniform film was obtained. The experiment was performed by first taking the background scan of air and spectrum resolution test. FTIR spectra of all samples were collected over the range from 400 to 4000 cm^{-1} with a 4 cm^{-1} resolution using an FTIR spectrometer (Tensor 27, Bruker, Borken, Germany). The baseline was automatically corrected and the spectra were normalized until the initial transmittance was 0.0 using PeakFit software (SYSTAT, Palo Alto, CA, USA). The measurements were performed in triplicate.

2.4.4. X-ray diffraction analysis

XRD analysis was conducted following the method of Azhar et al. (2021). The crystallinities of samples were determined using an X-ray diffractometer (Rigaku D/max2500, Rigaku Co., Ltd, Tokyo, Japan) with filtered Cu Kα radiation (λ = 0.1540 nm) at 40 kV and 40 mA. The diffraction angle 2θ was in the range of 5°–70°, the scanning step was 0.0262606° and the scan speed was 55° min^{-1}. Before the measurements, the sample powder was pressed into uniform flakes in the groove of the glass holder, which was placed in the sample chamber. The measurements were performed in duplicate. By applying the empirical method, the crystallinity index (CrI) was calculated as

$$\text{CrI}(\%) = (I_{200} - -I_{am})/I_{200} \times\ 100, \quad (2)$$

where I_{200} represented the intensity of the crystalline peak at approximately 22.4° and I_{am} was the intensity of the amorphous peak at approximately 18.32°.

2.4.5. NMR analysis

NMR analysis was performed following the method of Midhun Dominic et al. (2022) with some modifications. The samples were analyzed using a ^{13}C solid-state NMR instrument (JNM-ECZ400/600R, JEOL, Tokyo, Japan) equipped with an UltraShield Plus 400 MHz magnet and a 4 mm probe. The sample powder was packed into a 4 mm zirconia rotor. The parameters were set: spinning speed 8 kHz, the number of scans 8000, relaxation delay 5 s, CP contact time 2 ms, acquisition time 34 ms. The data were processed using the MestReNova9.0 software (Mestrelab Research S.L., Escondido, CA, USA). The measurements were performed in duplicate.

2.4.6. TGA evaluation

TGA and derivative thermogravimetry (DTG) were performed following the method of Masruchin et al. (2018). The samples were evaluated using a thermogravimetry analyzer (Pyris Diamond TG/DTA, PerkinElmer, Waltham, MA, USA). Beginning at room temperature, 5–10 mg of the sample was added to a Pt crucible and heated from 25 °C to 500 °C at a rate of 5 °C min^{-1} in air atmosphere, the weight curves during the heating process were recorded. The measurements were performed in triplicate.

2.5. Rheology of CNF suspensions

2.5.1. Rotational measurement

Rotational measurement was conducted following the method of Iotti et al. (2010) with some modifications. CNFs suspensions of 0.25 %, 0.5 %, 1.0 % and 1.5 % (w/v) were prepared by dispersing the CNFs powder into deionized water, and the ultrasonic (JY92-IIN, Scientz) treatment (65 W, 5 min) was performed to obtain uniform CNFs suspensions. Then, 15 mL of the suspension was placed in a container, and the viscosity of the suspensions was determined at 25 °C using a rheometer (MCR301, Anton Paar, Graz, Austria) equipped with a rotational viscometer (CC27-SN13078 probe type, $d = 0$ mm). The obtained viscosity was in a wide shear rate range of 0.1–1000 s^{-1}. The measurements were performed in triplicate.

2.5.2. Oscillation measurement

Oscillation measurement was conducted following the method of Yue and Qian (2018) with slight modifications. The dynamic rheological properties of the suspensions were determined using a rheometer (MCR301, Anton Paar) equipped with 50 mm diameter parallel plates (PP50-SN35731 probe type, $d = 1$ mm). A strain sweep (0.1 %–100 %) was performed at a frequency of 1 rad s^{-1} and 25 °C to determine the linear viscoelastic region. The temperature sweep tests were performed

at an angular frequency (ω) of 1 rad s^{-1} and a strain of 0.25 %. The frequency sweep tests were performed at a strain of 0.25 % and 25 °C, and the storage modulus (G') and loss modulus (G'') were recorded during the sweep. The measurements were performed in triplicate.

2.6. Statistical analysis

The data are expressed as mean ± standard deviation of triplicate experiments. Statistical analysis was performed using SPSS 23.0 (IBM, Armonk, NY, USA). The differences were considered significant at $p < 0.05$. The images were drawn using Origin 2022 (OriginLab, Northampton, MA, USA).

3. Results and discussion

3.1. Approximate compositions of potato residues and PCNFs

The main component of the potato residues was dietary fiber containing 24.86 % cellulose (based on the dry potato residues) (Table S1), which was an excellent raw material for preparing CNFs.

3.2. Isolation of PCNFs

To optimize the preparation parameters of PCNFs, the effects of different ultrasonic treatment time on the yield and zeta potential of PCNFs were compared, and the optimal ultrasonic treatment time (15 min) was selected. Then, the effects of different ultrasonic treatment powers on the yield and zeta potential of PCNFs were compared, and the optimal ultrasonic treatment power (125 W) was selected. After that, the effects of different homogenization cycles on the yield and zeta potential of PCNFs were compared, and the optimal number of homogenization cycles (four cycles) was selected. Finally, the effects of different homogenization pressures on the yield and zeta potential of PCNFs were compared, and the optimal homogenization pressure (40 MPa) was selected (Table S2).

Fig. 1 shows that with an increase in ultrasonic time, the PCNFs were gradually divided. Fig. 1(a) shows that when the ultrasonic time was less than 15 min, no division occurred, and the PCNFs were closely grouped, which made it difficult to determine the distribution range. At 15 min, the cellulose was divided entirely, with a diameter range of 20–80 nm (Table S2). At time greater than 15 min, the PCNFs were cut to smaller sizes, as shown in Fig. 1(a-iv, v), smaller PCNFs tended to aggregate (the red circles in Fig. 1), and the exposed charges on the surface were decreased, resulting in the zeta potential decrease (Wang et al., 2021). Fig. 1(b-i, ii and iii) presents the PCNFs cluster, which occurred because the ultrasonic power was too low to separate fibers completely. However, when the ultrasonic power was greater than 125 W, the PCNFs were broken into smaller sizes and tended to aggregate. From Fig. 1(c), when the homogenization cycles were less than 10 cycles, the AFM images showed obvious fibers, and in Fig. 1(c-iii, iv), no clusters were observed, and the diameter distribution range mainly was 15–70 nm (Table S2). Fig. 1(d) shows that when the pressure was 20 MPa or 40 MPa, the PCNFs appeared to be intertwined filaments of micron length [Fig. 1(d-i, ii)]. With a gradual increase in pressure, the PCNFs were cut

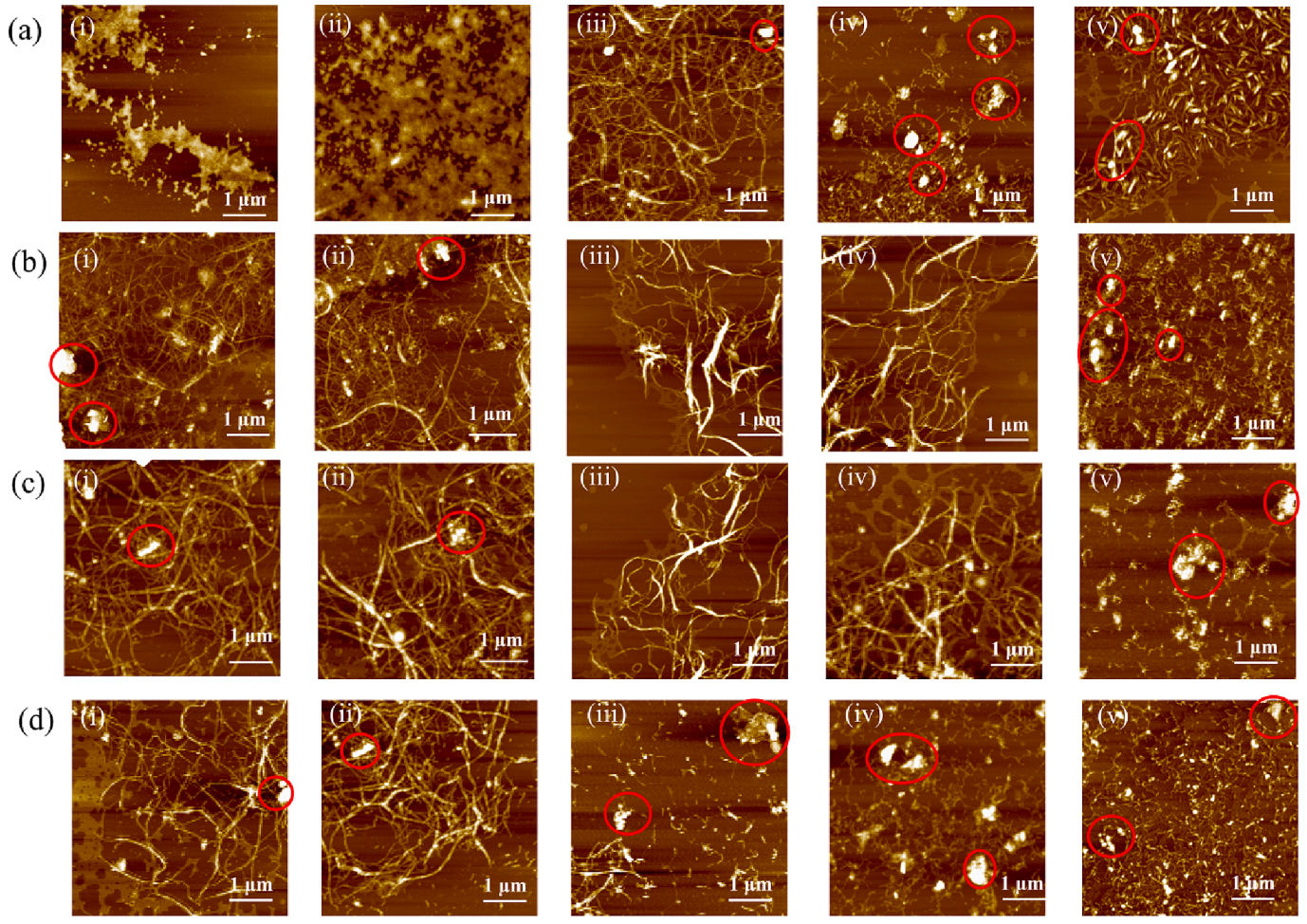

Fig. 1. The Atomic Force Microscopy image of PCNFs at the different ultrasonic time (a), ultrasonic powers (b), homogenization cycles (c) and homogenization pressures (d). Note: PCNFs, potato residues cellulose nanofibers. The red circles present the aggregation of CNFs.

off and shorter, tended to aggregate and the diameter distribution range decreased from 20–80 nm to 15–40 nm (Table S2).

Comprehensively considering the yield, zeta potential, and morphology of PCNFs, the optimal preparation parameters were selected as follows: ultrasonic treatment time, 15 min; ultrasonic power, 125 W; four homogenizations; and homogenization pressure, 40 MPa. Under the abovementioned conditions, the yield and zeta potential of PCNFs were 19.81 % (based on the potato residues) and −15.60 mV, respectively. Leite et al. (2017) prepared CNFs with a high-shear fluid processor microfluidizer. The yield was 69.11 % (based on cellulose), which was lower than the methods in this paper. The SEM images showed that the diameter distribution range of CNFs was 15–65 nm, which was similar to our results. Moron et al. (2017) prepared CNFs from cassava peelings and cassava bagasse by combining sulfuric acid and ultrasonic disintegration. The yield was 78 % (based on cellulose), the zeta potential of CNFs was −47.7 mV and the diameters were 2.33–5.37 nm. The zeta potential and diameter were lower than the results of our study, due to the SO_4^{2-} groups were attached to the CNFs' surface, which were more electronegative.

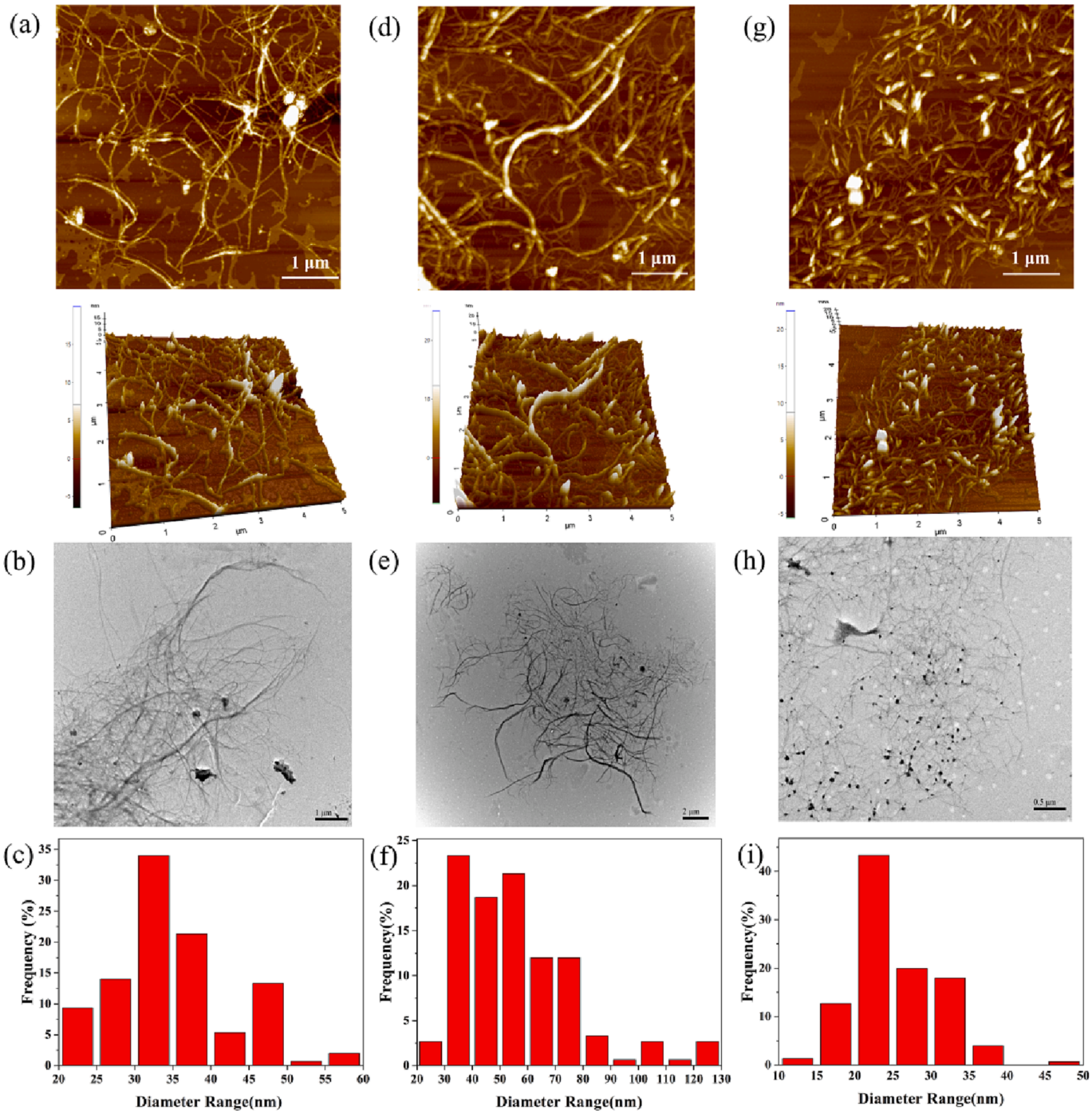

Fig. 2. The Atomic Force Microscopy, Transmission Electron Microscopy images, and diameter distribution of PCNFs, M-CNFs and TEMPO-CNFs. Note: (a-c), PCNFs. (d-f), M-CNFs. (g-i), TEMPO-CNFs. PCNFs, potato residues cellulose nanofibers. M-CNFs, commercial CNFs prepared by the mechanical method. TEMPO-CNFs, commercial CNFs prepared by TEMPO-mediated oxidation.

3.3. Characterization of PCNFs

3.3.1. Zeta potential and stability

Table S3 shows that the cellulose and CNFs all had negative surface charges. The zeta potential of the cellulose was −5.59 mV, whereas CNFs have more charges because with the larger specific surface area, more hydrogen bonds were carried on the CNFs' surface. In general, when the zeta potential is less negative than −30.0 mV, the suspension is considered to be stable (Wang et al., 2021). However, the zeta potentials of the PCNFs and M-CNFs were more negative than −30.0 mV at 0.1 % (w/v), indicating that the suspensions at 0.1 % (w/v) were unstable and prone to aggregation and settlement after storage for one day (Fig. S1). Conversely, the TEMPO-CNFs had a more negative zeta potential of −54.0 mV, indicating that the suspension had greater stability after storage for seven days. This may have occurred because TEMPO-CNFs were smaller in size and had a larger specific surface area, which exposed more hydrogen bonds. Furthermore, carboxyl groups were introduced in the process of preparing TEMPO-CNFs, which were more electronegative than hydroxyl groups (Masruchin et al., 2018).

3.3.2. Morphology

The AFM and TEM results showed the interlacing networks of PCNFs and M-CNFs (Fig. 2). The diameter distribution ranges of the PCNFs, M-CNFs and TEMPO-CNFs were 20–60, 20–130 and 10–50 nm, respectively (Fig. 2, Table S3). The diameters and lengths of TEMPO-CNFs were smaller because the oxidation properties of the TEMPO reagent accelerated the degradation process of cellulose. These results were similar to those reported by Mazela et al. (2020).

3.3.3. FTIR analysis

Fig. 3(a) shows that the variation in structural functional groups among the samples, shown by a broad absorption band in the range of 3200–3600 cm^{-1}, was attributed to the vibration of hydrogen-bonded hydroxyl groups. The peak at 2920 cm^{-1} was caused by the stretching vibration of saturated C—H (Lal & Mhaske, 2019). The presence of a peak at 1750 cm^{-1} in the potato residues was associated with the C═O stretching vibration of the acetyl and uronic ester groups. These groups are known to be present in pectin, hemicellulose and lignin (Nuruddin et al., 2016), however, no such peak was noted in the cellulose and PCNFs, indicating that the pectin, hemicellulose and lignin were removed completely. The band at 1619 cm^{-1} was assigned to the stretching vibration in the sodium carboxylate group (—COONa), indicating that the hydroxyl group at the C_6 of the cellulose was oxidized to the carboxyl group (Lal et al., 2019). The peak at 1519 cm^{-1} indicated the existence of aromatic rings, and thus, the presence of lignin. The FTIR absorption peak at 1430 cm^{-1} was attributed to the vibration of the —CH_2 bonds, which corresponded to the cellulose crystallinity band. The band at 890 cm^{-1} was attributed to the C—O—C stretching vibration of the β-1–4-glycosidic bond, which was considered to be an amorphous band (Nuruddin et al., 2016).

3.3.4. XRD analysis

The XRD results showed that the approximate positions of the diffraction peaks were $2\theta = 15.3°$, 16.4°, 22.5° and 34.2° [Fig. 3(b)], indicating the characteristic diffraction structure of cellulose I (native cellulose) (Azhar et al., 2021). The characteristic peaks of the sample appeared near 16.4°, 22.5° and 35°, indicating that the sample contained crystallized and amorphous structures. The PCNFs retained the characteristic peak of cellulose I β, indicating that the cellulose structure was not destroyed after high-pressure homogenization. Similar results have been achieved for nanocellulose extracted from sugar palms (Karina et al., 2020).

The CrIs of the potato residues and the cellulose extracted from potato residues were 11.26 % and 53.01 %, respectively. Because the lignin and the hemicellulose presented amorphous structures, they were removed, so the CrI of cellulose increased. After high-pressure homogenization, the CrI of the PCNFs was reduced to 35.44 % because the cellulose was destroyed by the homogenizer and became fibrous. This caused a shortened cellulose chain, and part of the crystallization area of the cellulose was destroyed (Xu et al., 2021). In addition, the crystallinities of the M-CNFs and TEMPO-CNFs were 73.48 % and 64.38 %, respectively, owing to the different raw materials. However, it is worth noting that the state of the sample had a significant effect on the CrI because potato residue powder was used in this study. The CrI obtained here from the powder was therefore greatly underestimated compared with that in the literature (Banvillet et al., 2021).

3.3.5. NMR analysis

Fig. 3(c) shows the NMR spectrum of potato residues, cellulose, PCNFs, M-CNFs and TEMPO-CNFs. The characteristic peaks corresponding to each carbon atom are 110 (C_1), 78–81 (C_2–C_3–C_5), 90–94 (C_4) and 68–71 ppm (C_6) (Midhun et al., 2022). For the PCNFs in our study, the same spectra were obtained for the chemical structure of cellulose extracted from potato residues. This indicated that the method used did not affect the structure of core cellulose. Moreover, M-CNFs and TEMPO-CNFs have sharper peaks, which were related directly to the higher crystallinity shown in Fig. 3(b). This result was attributed to the type and state of the raw material. A new peak appeared at 180.98 ppm, which correlated to the peak of the carboxyl group on the TEMPO-CNFs (Lal et al., 2019).

3.3.6. TGA evaluation

The onset temperatures (T_o) and maximum decomposition temperatures (T_{max}) of the samples are summarized in Table S4. As shown in Fig. 4(a), compared with the potato residues, the thermal stabilities of the cellulose and PCNFs were improved. When the temperature reached 230 °C, the substances began to degrade owing to the cleavage of the glycoside linkages of the cellulose (Dilamian et al., 2019). The T_{max} of the PCNFs (337 °C) was similar to that of the M-CNFs (338 °C), however, both were lower than that of the cellulose, at 340 °C. This reduction might correspond to the high surface area caused by the mechanical treatment, which accelerated the heat transfer rate and accordingly lowered the decomposition temperature (Dilamian et al., 2019). As shown in Fig. 4(b), the potato residues and M-CNFs showed a degradation peak around 470 °C, indicating that lignin exists there (Michelin et al., 2020); M-CNFs showed the peak possibly because the lignin was not removed completely. The absence of this specific degradation peak in PCNFs indicated that there was noncellulosic material in PCNFs, which was consistent with the results of FTIR. The weight losses of the PCNFs and M-CNFs were highest, at approximately 98 %, because the high-pressure homogenization shortened the fiber length and decreased the diameter, which facilitated thermal decomposition (Pakutsah & Aht-Ong, 2020). The results showed similar behavior to the degradation between the M-CNFs and PCNFs, even if the sizes of PCNFs were smaller than those of M-CNFs, indicating that the thermal stability was independent of the size. The TEMPO-CNFs began to degrade at 190 °C, the T_{max} was 269 °C, and the lowest weight loss was 73.08 %. Compared with the PCNFs and M-CNFs, the TEMPO-CNFs were the most easily decomposed because of the decarboxylation mechanism (the formation of sodium carboxylate groups in the TEMPO-CNFs) (Masruchin et al., 2018). The results of TGA and DTG showed CNFs prepared by the mechanical method were more thermally stable than those prepared with the TEMPO method.

3.4. Rheological properties of CNFs suspensions

3.4.1. Rotational measurement

The viscosities of all suspensions showed a rising trend with the increase in the concentrations of CNFs suspension (Fig. 5), indicating that the greater the number of CNFs, the more rigid the CNFs' network structure (Zhou et al., 2016). This phenomenon was attributed to the increased surface area of the nanofibers, allowing higher levels of

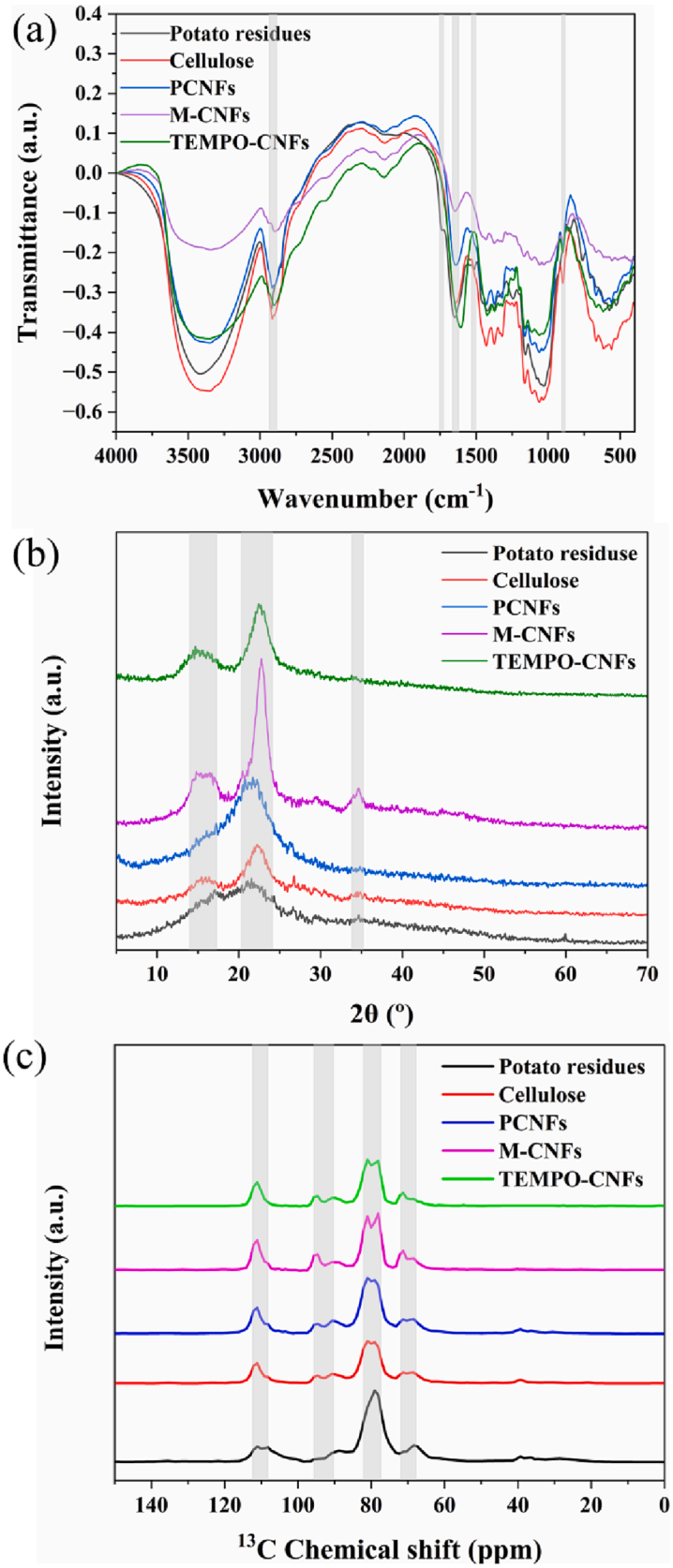

Fig. 3. Fourier transform infrared spectroscopy (a), X-ray diffraction (b), nuclear magnetic resonance spectroscopy (c) of potato residues, cellulose, PCNFs, M-CNFs, TEMPO-CNFs. Note: PCNFs, potato residues cellulose nanofibers. M-CNFs, commercial CNFs prepared by the mechanical method. TEMPO-CNFs, commercial CNFs prepared by TEMPO-mediated oxidation.

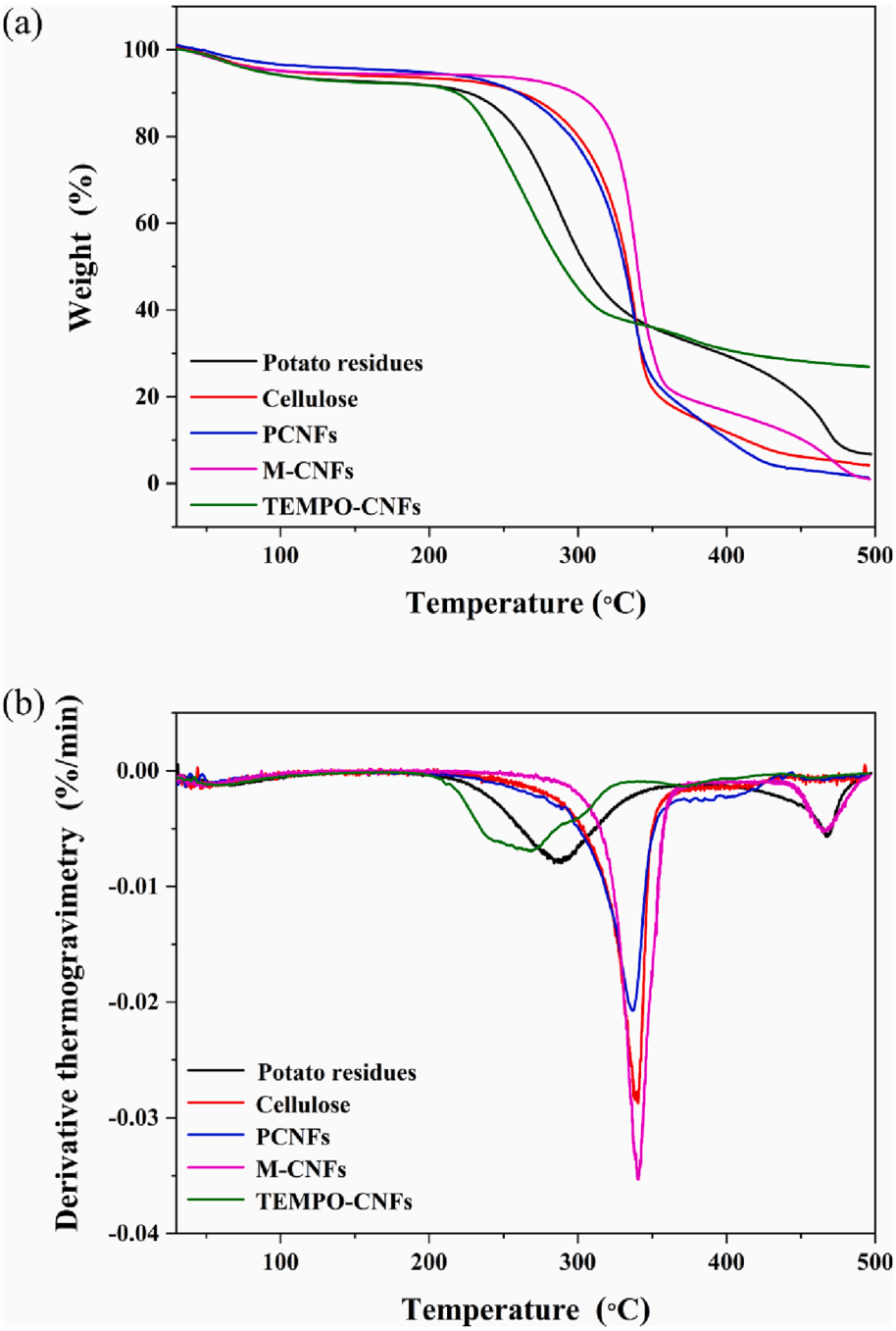

Fig. 4. Thermogravimetric analysis (a) and derivative thermogravimetry (b) curves of potato residues, cellulose, PCNFs, M-CNFs, TEMPO-CNFs. Note: PCNFs, potato residues cellulose nanofibers. M-CNFs, commercial CNFs prepared by the mechanical method. TEMPO-CNFs, commercial CNFs prepared by TEMPO-mediated oxidation.

interaction, as well as a suspension system of rigid polymeric chains oriented in the flow direction, which imparted a solid-like behavior (Gruneberger et al., 2014). With the increase in the shear rate, the viscosities of all CNFs suspensions decreased, which reflected the shear-thinning behavior and presented three distinct regions. As shown in Fig. 5(a, b), in the lower shear rate region, the viscosity decreased with the increased shear rate. This occurred because CNFs showed an ordered arrangement along the shear direction, resulting in a decrease in viscosity. In the middle shear rate region, the viscosity reached a plateau region and approached Newtonian behavior (Albornoz-Palma et al., 2020), indicating that the entangled CNFs molecules can resist the interference of shear force, and the viscosity no longer decreased. This was strongly correlated with the morphological characteristics, which were characterized by a highly entangled network between fibers and fiber bundles [Fig. 2(a, d)]. In the high-shear rate region, the higher shear force destroyed the hydrogen bonds between CNFs, resulting in a decrease in viscosity and an increase in fluidity (Chiulan et al., 2021; Czaikoski et al., 2020). Notably, for the PCNFs and M-CNFs, the viscosity of the 0.25 % (w/v) concentration suspensions increased when the shear rate exceeded 100 s^{-1}. The reason for the increase in viscosity may be that in suspensions with lower concentrations, the flow regime was no longer laminar and can gradually transform into turbulence. Under such conditions, the movement became more disordered in the fibers, which intertwined to form a network structure, thus, causing the viscosity to

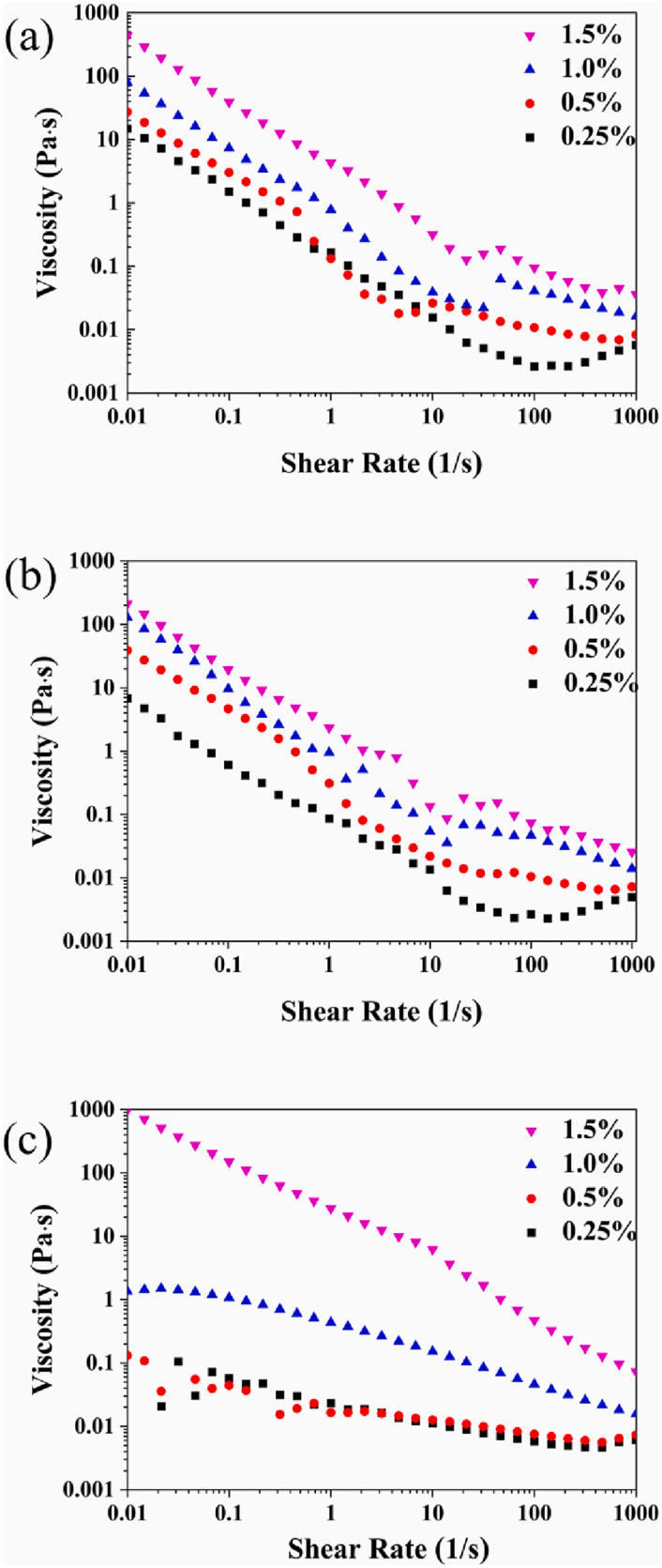

Fig. 5. The viscosity of PCNFs suspensions (a), M-CNFs suspensions (b), TEMPO-CNFs suspensions (c) as a function of shear rate. Note: PCNFs, potato residues cellulose nanofibers. M-CNFs, commercial CNFs prepared by the mechanical method. TEMPO-CNFs, commercial CNFs prepared by TEMPO-mediated oxidation.

increase slightly at a greater shear rate. Iotti et al. (2010) showed a similar three-region shear-thinning behavior of CNFs suspensions. Fig. 5 (c) shows the TEMPO-CNF curves of viscosity change with the shear rate. At concentrations less than 1.0 % (w/v), irregular viscosity change appeared in the low shear rate region, which may be attributed to the inertial effects usually present in rheometers. The PCNFs and M-CNFs showed similar viscosity properties, indicating that the viscosity of CNFs may be dependent on the preparation method.

3.4.2. Oscillation measurement

In general, dynamic strain sweeps were required to determine the dependence of strain on sample modulus to identify the linear viscoelastic region. As shown in Fig. S2(a, b), when the strain amplitude value was less than 1.0 %, the G' curves of PCNFs suspensions and M-CNFs suspensions were maintained, however, for TEMPO-CNFs suspensions with 0.5 % (w/v) and 1.0 % (w/v) concentration [Fig. S2(c)], the G' were maintained when the strain amplitude value was less than 10 %. Therefore, for subsequent measurements of temperature and frequency sweeps, the strain amplitude was selected to be 0.25 % except for TEMPO-CNFs suspensions at 0.25 % (w/v) and 0.5 % (w/v). This was because the curve [Fig. S2(c)] fluctuated in the range of 0.1 %–1.0 %, the linear viscoelastic range might not be determined for such low concentrations, therefore, the temperature and frequency sweeps were not performed with 0.25 % (w/v) and 0.5 % (w/v) TEMPO-CNFs suspensions.

Fig. 6(a–c) shows the variations in G' and G'' with temperatures of 25–90 °C. With an increase in concentration, G' and G'' showed an increasing trend. These results were similar to the values reported by Yue et al. (2018), who isolated CNFs from coir fibers. As shown in Fig. 6 (a, b), the changes in G' and G'' were temperature independent for the PCNFs suspensions and the M-CNFs suspensions, indicating the thermal motion cannot destroy the hydrogen bonds between nanofibers, causing the PCNFs and M-CNFs suspensions to show excellent viscoelasticity (Yu et al., 2021). Moreover, the G' was always higher than the G'', indicating that the PCNFs and M-CNFs suspensions exhibited elastic behavior. Fig. 6(c) shows that the G' and G'' increased with increasing temperature. This indicated that the effect of the thermal motion was stronger than the hydrogen bonding and mechanical resistance caused by cross-linking between nanofibers, which might be strongly related to the small sizes of the TEMPO-CNFs. For the 1.0 % (w/v) TEMPO-CNFs suspension, when the temperature was below 50 °C, G' was close to G'', with a higher temperature the G' was clearly greater than the G'', indicating that high temperature facilitated the transition to viscoelastic.

As shown in Fig. 6(d, e), PCNFs suspensions and M-CNFs suspensions at 0.25 % (w/v) and 0.5 % (w/v) showed strong frequency dependence. As the concentrations increased, the PCNFs suspensions and M-CNFs suspensions became frequency insensitive, indicating that PCNFs suspensions and M-CNFs suspensions with higher concentrations were stable and were not affected by frequency change. This difference indicated that the formation rate of intrinsic networks by hydrogen bonds will be affected by high frequency in the PCNFs suspensions and M-CNFs suspensions at low concentrations (Chen et al., 2013). Moreover, the G' was always larger than the G'', which indicated that the PCNFs suspensions and M-CNFs suspensions showed typical characteristics of rigid colloidal particles and dominant elastic behavior (Pakutsah & Aht-Ong, 2020). When the concentration was 0.25 % (w/v) and 0.5 % (w/v), the PCNFs suspensions and M-CNFs suspensions showed that G' was not stable at a higher angle frequency value, possibly because the flow regime was no longer laminar. However, when the concentration of PCNFs suspensions and M-CNFs suspensions was greater than 0.5 % (w/v), the suspensions were insensitive during the entire frequency sweep. This may be attributed to the presence of more fibers at higher concentrations, which formed a network structure with sufficient stability to resist the frequency effect because the rate of destroying and rebuilding the network structure can be balanced (Chen et al., 2013). As for TEMPO-CNFs suspensions, Fig. 6(f) shows the trend of frequency dependence that diminished as the concentration increased. For the TEMPO-CNFs suspension at 1.0 % (w/v), the value of G'' exceeded that of G' at 20 rad s^{-1}, and the suspension changed from viscoelastic to viscofluid. This may have occurred because the contents

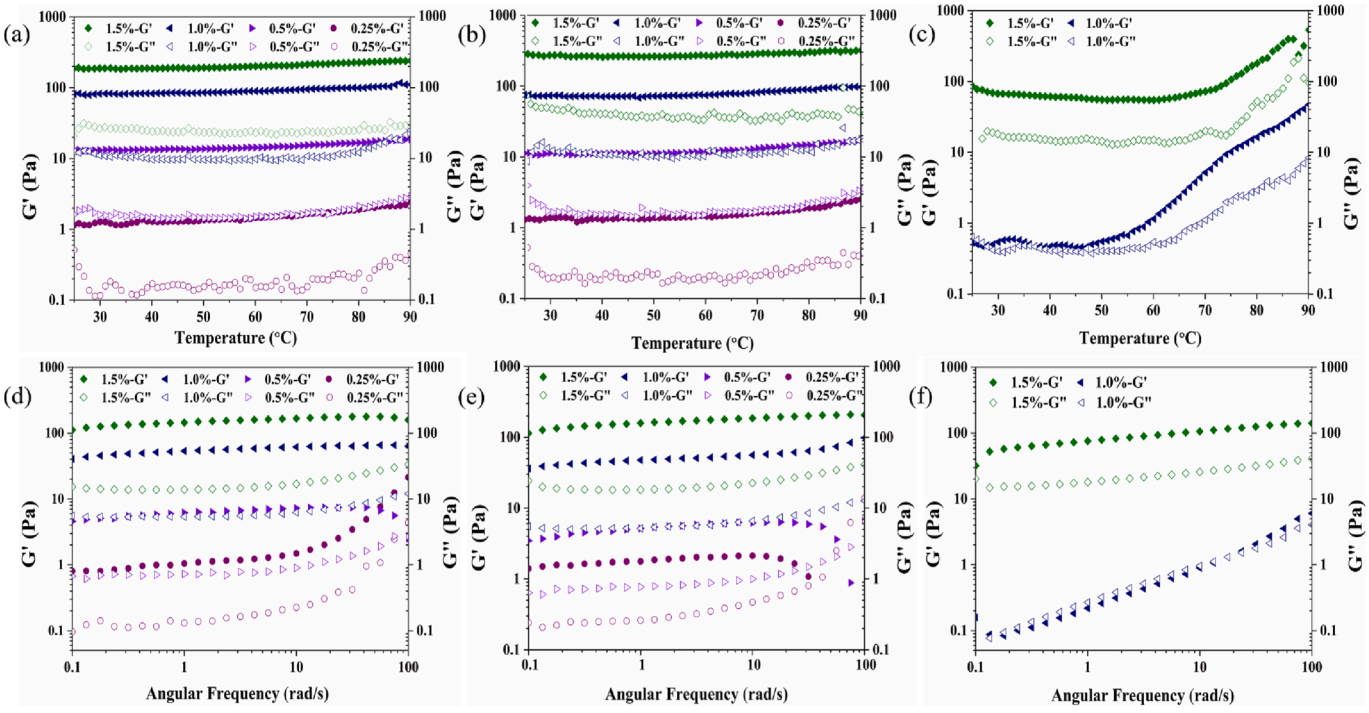

Fig. 6. Storage modulus (G', filled symbols) and loss modulus (G'', open symbols) as a function of the temperature of angular frequency. Note: (a, d), PCNFs suspensions. (b, e), M-CNFs suspensions. (c, f), TEMPO-CNFs suspensions. PCNFs, potato residues cellulose nanofibers. M-CNFs, commercial CNFs prepared by the mechanical method. TEMPO-CNFs, commercial CNFs prepared by TEMPO-mediated oxidation.

and aspect ratio were too low to form a stable network structure.

In addition, tan δ is equal to the ratio of G'' to G'. As shown in Fig. S3, the tan δ values of the PCNFs suspension, M-CNFs suspension and TEMPO-CNFs suspension with 1.5 % (w/v) were 0.1–0.3. This indicated that they were mainly in the elastic rheological state, which was consistent with the results of Yu et al. (2021). However, Fig. S3(c) shows that the tan δ of 1.0 % (w/v) TEMPO-CNFs suspension was greater than 1, indicating that 1.0 % (w/v) TEMPO-CNFs suspension was not stable.

4. Conclusion

In summary, PCNFs were prepared using residues generated during potato starch processing by ultrasonication combined with high-pressure homogenization. The highest yield, 19.81 %, was achieved with ultrasonic treatment at 125 W for 15 min and high-pressure homogenization treatment at 40 MPa for four cycles. The mechanical force caused the cellulose in the potato residues to be broken into PCNFs. Although this did not affect the chemical structure of the cellulose, the destruction of part of the crystalline region resulted in a decrease in the CrI from 53.01 % to 35.44 %. Moreover, the maximum thermal degradation temperature of the PCNFs increased to 337 °C compared with that of the potato residues (283 °C). The PCNFs suspensions exhibited rigid colloidal particle behavior in the linear viscoelastic range, predominantly elastic behavior (tan δ values were 0.1–0.3). When the concentration of PCNFs was 1.5 % (w/v), the initial viscosity, G' of frequency sweep and G' of temperature sweep were 438 Pa·s, 112 Pa and 187 Pa, respectively. Meanwhile, PCNFs suspensions showed excellent temperature-independent rheological stability, and frequency insensitivity when the concentration was higher than 0.25 % (w/v). These results indicated that the potato residues generated from starch processing are a good source for producing value-added products such as CNFs, which have great potential in a variety of industrial applications.

CRediT authorship contribution statement

Xiaown Liu: Formal analysis, Investigation, Data curation, Writing – original draft. **Hongnan Sun:** Visualization, Validation, Writing – review & editing, Supervision. **Taihua Mu:** Funding acquisition, Conceptualization, Supervision. **Mei Li:** Resources, Writing - review & editing.

Declaration of Competing Interest

The authors declare that they have no known competing financial interests or personal relationships that could have appeared to influence the work reported in this paper.

Data availability

Data will be made available on request.

Acknowledgments

The authors gratefully acknowledge the Central Public-interest Scientific Institution Basal Research Fund (S2022JBKY-14), and the Science and Technology Innovation Project of Chinese Academy of Agricultural Sciences (CAAS-ASTIP-202X-IFST).

Appendix A. Supplementary data

Supplementary data to this article can be found online at https://doi.org/10.1016/j.foodchem.2023.135675.

References

AOAC Official Method, 1999 AOAC Official Method 930.15. Dry Matter on Oven Drying for Feeds, First Action 1930. AOAC Official Method 954.02. Fat (Crude) or Ether Extract in Pet Food, First Action 1954 Final Action 1977. AOAC Official Method 976.05. Protein (Crude) in Animal Feed and Pet Food, First Action 1976 Final Action 1977. AOAC Official Method 942.05. Ash of Animal Feed, First Action 1942. AOAC Official Method 991.43. Total, soluble, and insoluble dietary fiber in foods, first action 1991 and final action 1994. Washington, DC: Association of Official Analytical Chemists.

Albornoz-Palma, G., Betancourt, F., Mendonca, R. T., Chinga-Carrasco, G., & Pereira, M. (2020). Relationship between rheological and morphological characteristics of cellulose nanofibrils in dilute dispersions. *Carbohydrate Polymers, 230*, Article 115588. https://doi.org/10.1016/j.carbpol.2019.115588

Arvidsson, R., Nguyen, D., & Svanstrom, M. (2015). Life cycle assessment of cellulose nanofibrils production by mechanical treatment and two different pretreatment processes. *Enviromental Science & Technology, 49*(11), 6881–6890. https://doi.org/10.1021/acs.est.5b00888

Azhar, S. W., Xu, F., & Qiu, Y. (2021). Evaluation and characterization of cellulose nanofibers from flaxseed fiber bundles. *AATCC Journal of Research, 8*(4), 8–14. https://doi.org/10.14504/ajr.8.4.2

Banvillet, G., Depres, G., Belgacem, N., & Bras, J. (2021). Alkaline treatment combined with enzymatic hydrolysis for efficient cellulose nanofibrils production. *Carbohydrate Polymers, 255*, Article 117383. https://doi.org/10.1016/j.carbpol.2020.117383

Chen, P., Yu, H., Liu, Y., Chen, W., Wang, X., & Ouyang, M. (2013). Concentration effects on the isolation and dynamic rheological behavior of cellulose nanofibers via ultrasonic processing. *Cellulose, 20*(1), 149–157. https://doi.org/10.1007/s10570-012-9829-7

Chiulan, I., Panaitescu, D. M., Radu, E. R., Vizireanu, S., Satulu, V., Bita, B., … Raditoiu, V. (2021). Influence of TEMPO oxidation on the properties of ethylene glycol methyl ether acrylate grafted cellulose sponges. *Carbohydrate Polymers, 272*, Article 118458. https://doi.org/10.1016/j.carbpol.2021.118458

Czaikoski, A., da Cunha, R. L., & Menegalli, F. C. (2020). Rheological behavior of cellulose nanofibers from cassava peel obtained by combination of chemical and physical processes. *Carbohydrate Polymers, 248*, Article 116744. https://doi.org/10.1016/j.carbpol.2020.116744

Dilamian, M., & Noroozi, B. (2019). A combined homogenization-high intensity ultrasonication process for individualizaion of cellulose micro-nano fibers from ricestraw. *Cellulose, 26*(10), 5831–5849. https://doi.org/10.1007/s10570-019-02469-y

Gruneberger, F., Kunniger, T., Zimmermann, T., & Arnold, M. (2014). Rheology of nanofibrillated cellulose/acrylate systems for coating applications. *Cellulose, 21*(3), 1313–1326. https://doi.org/10.1007/s10570-014-0248-9

Hamawand, I., Seneweera, S., Kumarasinghe, P., & Bundschuh, J. (2020). Nanoparticle technology for separation of cellulose, hemicellulose and lignin nanoparticles from lignocellulose biomass: A short review. *Nano-Structures & Nano-Objects, 24*, Article 100601. https://doi.org/10.1016/j.nanoso.2020.100601

Hongrattanavichit, I., & Aht-Ong, D. (2020). Nanofibrillation and characterization of sugarcane bagasse agro-waste using water-based steam explosion and high-pressure homogenization. *Journal of Cleaner Production, 277*. https://doi.org/10.1016/j.jclepro.2020.123471

Iotti, M., Gregersen, Ø. W., Moe, S., & Lenes, M. (2010). Rheological studies of microfibrillar cellulose water dispersions. *Journal of Polymers and the Environment, 19*(1), 137–145. https://doi.org/10.1007/s10924-010-0248-2

Karina, M., Satoto, R., Abdullah, A. H. D., & Yudianti, R. (2020). Properties of Nanocellulose obtained from sugar palm (Arenga pinnata) fiber by acid hydrolysis in combination with high-pressure homogenization. *Cellulose Chemistry and Technology, 54*(1–2), 33–38. https://doi.org/10.35812/CelluloseChemTechnol.2020.54.04

Kumari, P., & Meena, A. (2021). Application of enzyme-mediated cellulose nanofibers from lemongrass waste for the controlled release of anticancer drugs. *Environmental Science and Pollution Research, 28*(34), 46343–46355. https://doi.org/10.1007/s11356-020-08358-3

Lal, S. S., & Mhaske, S. T. (2019). TEMPO-oxidized cellulose nanofiber/kafirin protein thin film crosslinked by Maillard reaction. *Cellulose, 26*(10), 6099–6118. https://doi.org/10.1007/s10570-019-02509-7

Leite, A. L. M. P., Zanon, C. D., & Menegalli, F. C. (2017). Isolation and characterization of cellulose nanofibers from cassava root bagasse and peelings. *Carbohydrate Polymers, 157*, 962–970. https://doi.org/10.1016/j.carbpol.2016.10.048

Li, M. C., Wu, Q. L., Song, K. L., Lee, S., Qing, Y., & Wu, Y. Q. (2015). Cellulose nanoparticles: Structure-morphology-rheology relationships. *ACS Sustainable Chemistry & Engineering, 3*(5), 821–832. https://doi.org/10.1021/acssuschemeng.5b00144

Ma, M. M., Mu, T. H., Sun, H. N., Zhang, M., Chen, J. W., & Yan, Z. B. (2015). Optimization of extraction efficiency by shear emulsifying assisted enzymatic hydrolysis and functional properties of dietary fiber from deoiled cumin (Cuminum cyminum L.). *Food Chemistry, 179*, 270–277. https://doi.org/10.1016/j.foodchem.2015.01.136

Ma, Q., Ma, Z., Wang, W., Mu, J., Liu, Y., Wang, J., … Sun, J. (2022). The effects of enzymatic modification on the functional ingredient – Dietary fiber extracted from potato residue. *LWT - Food Science and Technology, 153*. https://doi.org/10.1016/j.lwt.2021.112511

Masruchin, N., Park, B. D., & Lee, J. M. (2018). Surface modification of TEMPO-oxidized cellulose nanofibrils for composites to give color change in response to pH level. *Cellulose, 25*(12), 7079–7090. https://doi.org/10.1007/s10570-018-2072-0

Mazela, B., Perdoch, W., Peplinska, B., & Zielinski, M. (2020). Influence of chemical pretreatments and ultrasonication on the dimensions and appearance of cellulose fibers. *Materials, 13*(22). https://doi.org/10.3390/ma13225274

Michelin, M., Gomes, D. G., Romani, A., Polizeli, M., & Teixeira, J. A. (2020). Nanocellulose production: Exploring the enzymatic route and residues of pulp and paper industry. *Molecules, 25*(15). https://doi.org/10.3390/molecules25153411

Midhun Dominic, C. D., Raj, V., Neenu, K. V., Begum, P. M. S., Formela, K., Saeb, M. R., … Parameswaranpillai, J. (2022). Chlorine-free extraction and structural characterization of cellulose nanofibers from waste husk of millet (Pennisetum glaucum). *International Journal of Biological Macromolecules, 206*, 92–104. https://doi.org/10.1016/j.ijbiomac.2022.02.078

Moron Pereira Leite, Zanon, C. D., & Menegalli, F. C. (2017). Isolation and characterization of cellulose nanofibers from cassava root bagasse and peelings. *Carbohydrate Polymers, 157*, 962–970. https://doi.org/10.1016/j.carbpol.2016.10.048.

Nuruddin, M., Hosur, M., Uddin, M. J., Baah, D., & Jeelani, S. (2016). A novel approach for extracting cellulose nanofibers from lignocellulosic biomass by ball milling combined with chemical treatment. *Journal of Applied Polymer Science, 133*(9). https://doi.org/10.1002/app.42990

Pakutsah, K., & Aht-Ong, D. (2020). Facile isolation of cellulose nanofibers from water hyacinth using water-based mechanical defibrillation: Insights into morphological, physical, and rheological properties. *International Journal of Biological Macromolecules, 145*, 64–76. https://doi.org/10.1016/j.ijbiomac.2019.12.172

Pandey, A. (2021). Pharmaceutical and biomedical applications of cellulose nanofibers: A review. *Environmental Chemistry Letters, 19*(3), 2043–2055. https://doi.org/10.1007/s10311-021-01182-2

Scharf, R., Wang, R., Maycock, J., Ho, P., Chen, S., & Orfila, C. (2020). Valorisation of potato (Solanum tuberosum) peel waste: Extraction of fibre, monosaccharides and uronic acids (vol 53, pg 631, 2019). *Waste and Biomass Valorization, 11*(8), 4571. https://doi.org/10.1007/s12649-019-00686-x

Serra, A., Gonzalez, I., Oliver-Ortega, H., Tarres, Q., Delgado-Aguilar, M., & Mutje, P. (2017). Reducing the amount of catalyst in TEMPO-oxidized cellulose nanofibers: Effect on properties and cost. *Polymers, 9*(11). https://doi.org/10.3390/polym9110557

Waliullah, M. H., Mu, T., & Ma, M. (2021). Recovery of total, soluble, and insoluble dietary fiber from potato (Solanum tuberosum) residues and comparative evaluation of their structural, physicochemical, and functional properties. *Journal of Food Processing, 45*(7). https://doi.org/10.1111/jfpp.15650

Wang, J., Xu, J., Zhu, S., Wu, Q., Li, J., Gao, Y., … Chen, K. (2021). Preparation of nanocellulose in high yield via chemi-mechanical synergy. *Carbohydrate Polymers, 251*, Article 117094. https://doi.org/10.1016/j.carbpol.2020.117094

Widiarto, S., Pramono, E., Rochliadi, A., & Arcana, I. M. (2019). Cellulose nanofibers preparation from cassava peels via mechanical disruption. *Fibers, 7*(5). https://doi.org/10.3390/fib7050044

Wijesinha-Bettoni, R., & Mouille, B. (2019). The contribution of potatoes to global food security, nutrition and healthy diets. *American Journal of Potato Research, 96*(2), 139–149. https://doi.org/10.1007/s12230-018-09697-1

Xie, J. L., Hse, C. Y., De Hoop, C. F., Hu, T. X., Qi, J. Q., & Shupe, T. F. (2016). Isolation and characterization of cellulose nanofibers from bamboo using microwave liquefaction combined with chemical treatment and ultrasonication. *Carbohydrate Polymers, 151*, 725–734. https://doi.org/10.1016/j.carbpol.2016.06.011

Xu, S., Huo, D., Wang, K., Yang, Q., Hou, Q., & Zhang, F. (2021). Facile preparation of cellulose nanofibrils (CNFs) with a high yield and excellent dispersibility via succinic acid hydrolysis and NaClO(2) oxidation. *Carbohydrate Polymers, 266*, Article 118118. https://doi.org/10.1016/j.carbpol.2021.118118

Yu, B., Zeng, X., Wang, L., & Regenstein, J. M. (2021). Preparation of nanofibrillated cellulose from grapefruit peel and its application as fat substitute in ice cream. *Carbohydrate Polymers, 254*, Article 117415. https://doi.org/10.1016/j.carbpol.2020.117415

Yue, D., & Qian, X. (2018). Isolation and rheological characterization of cellulose nanofibrils (CNFs) from coir fibers in comparison to wood and cotton. *Polymers, 10*(3). https://doi.org/10.3390/polym10030320

Zai, Z., Yan, M., Shi, C., Zhang, L., Lu, H., Xiong, Z., & Ma, J. (2022). Cellulose nanofibrils (CNFs) in uniform diameter: Capturing the impact of carboxyl group on dispersion and Re-dispersion of CNFs suspensions. *International Journal of Biological Macromolecules, 207*, 23–30. https://doi.org/10.1016/j.ijbiomac.2022.03.001

Zhou, L., He, H., Li, M. C., Song, K. L., Cheng, H. N., & Wu, Q. L. (2016). Morphological influence of cellulose nanoparticles (CNs) from cottonseed hulls on rheological properties of polyvinyl alcohol/CN suspensions. *Carbohydrate Polymers, 153*, 445–454. https://doi.org/10.1016/j.carbpol.2016.07.119

FAO (Food and Agriculture Organization of the United Nations). FAOSTAT Statistics Database. http://www.fao.org/faostat/en/#data/QC.